Asian Journal of Chemistry; Vol. 31, No. 12 (2019), 2941-2954

ASIAN JOURNAL OF CHEMISTRY

https://doi.org/10.14233/ajchem.2019.22308

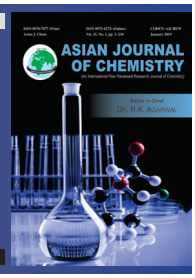

DNA/BSA Binding, Molecular Docking, Nuclease Activity and Cytotoxicity Studies of Hydrazide Based Schiff Base Complexes

MUTHIAH CHINNASAMY and ANDY RAMU*

Department of Inorganic Chemistry, School of Chemistry, Madurai Kamaraj University, Madurai-625021, India

*Corresponding author: E-mail: ramumku@yahoo.co.in

Received: 2 July 2019; *Accepted*: 27 August 2019; *Published online*: 16 November 2019; AJC-19645

A new series of hydrazide based Schiff base metal Cu(II)/Zn(II) complexes of the type $[Cu(L1\text{-}L4)_2]$ and $[Zn(L1\text{-}L4)_2]$ has been synthesized and characterized by various analytical and spectral techniques. The proposed geometry of metal complexes, square planar for Cu^{2+} ion and tetrahedral for Zn^{2+} ion was confirmed by the spectral and analytical results. DNA interaction with metal complexes was explored by spectral and molecular docking analysis. The results obtained indicates that Cu(II)/Zn(II) complexes interaction with DNA *via* an intercalative binding mode and its respective intrinsic binding constant (K_b) was found in the order of **7 > 8 > 5 > 6 > 3 > 4 > 1 > 2**. Further, similar interactions of these metal complexes with BSA were found in the same order of binding constant. Furthermore, the complexes showed moderate cleavage ability with pUC19 DNA. Cytotoxicity studies confirmed the biological importance of the Schiff base complexes.

Keywords: Schiff base metal complexes, Antibacterial activity, Cytotoxicity, DNA/BSA binding, DNA docking.

INTRODUCTION

In pharmacology, modern chemists and biologists are attracted to transition metal complexes and their interaction studies with various biomolecules/biosystem [1-3]. Specifically, DNA binding, DNA cleavage and anticancer ability of the coordinated metal complexes are notable research area in the drug design [4]. DNA is the prime intracellular targets for anti-cancer drugs and essential behind the discovery of new and effective drugs towards many contagious diseases in human [5-7]. At present, inorganic transition metal complexes are used effectively in the treatment of several cancers as chemotherapy medicine in order to overcome the side effects occurs during radiotherapy [8]. These problems and challenges have stirred a curiosity to chemists and biologist to develop new medicines [9-11].

Schiff bases with nitrogen, oxygen and sulphur hetero-atoms and their coordination compounds with various second and third transition metals are the main themes of the present research [12,13]. Specifically, hydrazone derivatives play a crucial role in certain physiological functions of the drug [14]. Further, hydrazone ligands coordination with various metal II/III ions [15,16] revealed a wide range of biological functions and pharmaceutical activities, which includes antifungal, anti-bacterial, antiviral, antioxidant, anticancer, anti-tuberculosis and anti-inflammatory activities, *etc*. [17-19].

Among many, copper and zinc metals are the most essential metals in human anatomical system. Due to low toxicity, it may be used as the substitutes for various metal complexes in the cancer medicines [20-22]. Copper(II) and zinc(II) complexes were studied for their biological activity, anticancer activity and some of them were found to be active both in *in-vivo* and *in-vitro* models [23]. Cu(II) complexes have a unique preference for covalent mode of binding *via* N7 of guanine and Zn(II) complexes efficiently involved in diagnosing the N3 of thymine nucleobase [24,25]. Similarly, bovine serum albumin (BSA) have been studied widely in drug tests as a replacement for human serum albumin (HSA) [26,27], because it has been considered structurally and functionally homology with human serum albumin. Serum albumins binding to metallo drugs perform an important role in their distribution and metabolism [28,29]. The present study is to explore synthesis and structural characterization of new hydrazide based transition Cu(II)/Zn(II) complexes and their interaction with DNA/BSA

binding, along with molecular docking, antioxidant, antibacterial and cytotoxicity activities.

EXPERIMENTAL

All chemicals, solvents and reagents used in this study were of AR grade. (4-Pyrrolidine-1-yl)benzaldehyde, hydrazide derivatives (Sigma-Aldrich), tetrabutylammonium perchlorate (TBAP) (Fluka) were obtained and used without any further purification. Tris-HCl, sodium chloride, bovine serum albumins (BSA) and herring serum-DNA (SRL) was used as received. 3-(4,5-Dimethylthiazol-2-yl)-2,5-diphenyltetrazolium bromide (MTT) reagent grade was found to be Calbiochem and used as received.

Physical measurements: Elemental analysis (C, H and N) were carried out by using elemental analyzer (Vario III). FT-IR spectra of ligands (**L1-L4**) and its metal complexes (**1-8**) were recorded by using dual beam infrared spectrophotometer (TFNICOLET6700) in the range of 4000-400 cm^{-1}. The ^{1}H, ^{13}C NMR spectra were obtained from NMR (Bruker 300 MHz, 75 MHz) spectrometer. ESI mass spectroscopic analyses were carried out in mass spectrometer LCQ Fleet (Thermo Fisher Instruments Limited, USA). Electronic absorption spectra of the Schiff base ligands and metal complexes were recorded by using UV-Visible spectrophotometer (JASCO V-550). The titration spectra were recorded in solution by using fluorescence spectrophotometer (Agilent Cary Eclipse-8000). The surface morphology of HeLa cancer cell line was premeditated by using scanning electron microscopy (SEM, VEGA 3, TESCAN).

Synthesis of hydrazide based Schiff base ligands: 4-(Pyrrolidino-1-yl)benzaldehyde (0.1mmol) and 0.1 mmol of several substituted hydrazine (phenylhydrazine, 4-methylphenyl hydrazide, furanhydrazide and thiophenehydrazide) were soluble in methanol and refluxed for about 1- 4 h until the completion of the reaction. The reaction was monitored by TLC. Afterward, the reaction mixtures were filtered washed several times with cold methanol and further purified petroleum ether. The solid ligands (**L1-L4**) was recrystallized in cold methanol and dried with P_4O_{10} under vacuum condition (**Scheme-I**).

N′-(4-(Pyrrolidin-1-yl)benzylidene)benzohydrazide (L1): Yield: 92 %. m.p.: 144 ºC, colour: yellow. Anal. calcd. (found) % for $C_{18}H_{19}N_3O$: C, 73.69 (73.45); H, 6.53 (6.38); N, 14.32 (14.1). FT-IR bands (KBr, cm^{-1}): 1616 ν(HC=N); 3070, 2821 ν(H_2C-CH_2); 1626 ν(-CO), 3192 ν(-NH). ^{1}H NMR (300 MHz, $CDCl_3$, ppm): δ 8.25 (s, 1H, HC=N-); δ 6.54-7.79 (m, 10H, Ar-H); δ 2.03, 3.34 (q, q, 8H, CH_2); δ 9.71(s, 1H, NH), δ 2.73 (q, 4H, DMSO-d_6 solvent). UV-vis (DMSO, nm): 262, 362. ESI-MS: Found *m/z* = 294.30 [M+H] (calcd value: *m/z* = 293).

4-Methyl-N′-(4-(pyrrolidin-1-yl)benzylidene)benzohydrazide (L2): Yield: 90 %. m.p.: 121 ºC, colour: yellow. Anal. calcd. (found) % for $C_{19}H_{21}N_3O$: C, 74.24 (74.16); H, 6.89 (6.71); N, 13.67 (13.28). FT-IR bands (KBr, cm^{-1}): 1607 ν(HC=N); 2939, 2860 ν(H_2C-CH_2); 1637 ν(-CO); 3269 ν(-NH). ^{1}H NMR (300 MHz, $CDCl_3$, ppm): δ 8.27 (s, 1H, HC=N); δ 6.53-7.84 (m, 10H, Ar-H); δ 2.02, 3.34 (qq, 8H, -CH_2), δ 2.41 (s, 1H, -CH_3), δ 10.86 (s, 1H, -NH), δ 3.03 (m,14H, DMSO-d_6 solvent), δ 4.74, δ1.73 (DCM, acetone). UV-vis (DMSO, nm):

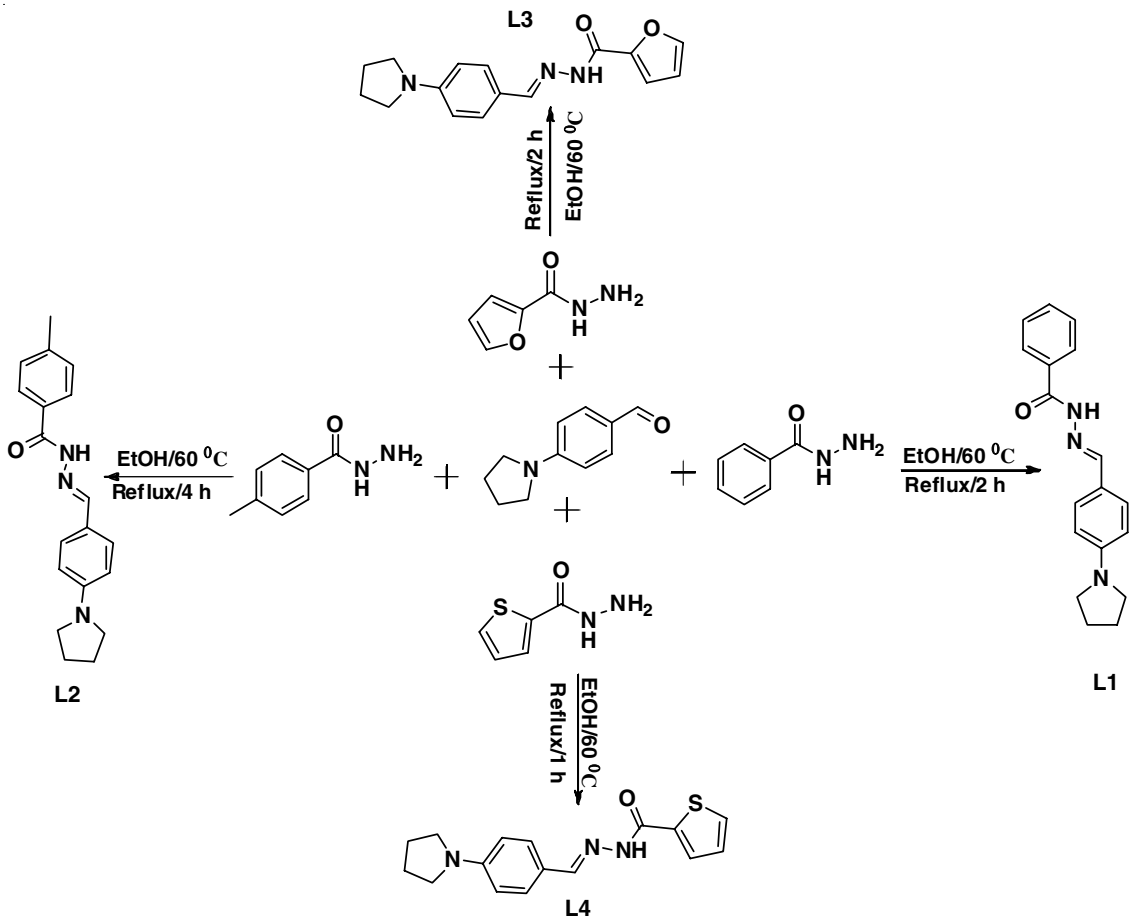

Scheme-I: Synthetic route for the Schiff base ligands (**L1-L4**)

259, 361. ESI-MS: Found *m/z* = 306.10 [M-H] (calcd value: *m/z* = 307).

N′-(4-(Pyrrolidin-1-yl)benzylidene)furan-2-carbohydrazide (L3): Yield: 87 %, m.p.: 114 ºC, colour: yellow. Anal. calcd. (found) % for $C_{16}H_{17}N_3O_2$: C, 67.83 (67.24); H, 6.05 (6.04); N, 14.83 (14.08). FTIR bands (KBr, cm^{-1}): 1646 ν(HC=N); 3163, 2965 ν(H_2C-CH_2); 1646 ν(-CO); 3472 ν(-NH). ^{1}H NMR (300 MHz, $CDCl_3$, ppm): δ 8.06 (s, 1H, HC=N); δ 6.53-7.67(m, 8H, Ar-H); δ 2.03, 3.35 (qq, 8H, -CH_2), δ 9.21 (s, 1H, -NH), δ 2.18 (m,7H, DMSO-d_6 solvent), δ 2.81 (acetone). UV-vis (DMSO, nm): 248, 366. ESI-MS: Found *m/z* = 283.08 [M+H] (calcd value: *m/z* = 283).

N′-(4-(Pyrrolidin-1-yl)benzylidene)thiophene-2-carbohydrazide (L4): Yield: 89 %. m.p.: 104 ºC, colour: yellow. Anal. calcd. (found) % for $C_{16}H_{17}N_3OS$: C, 64.19 (64.04); H, 5.72 (5.36); N, 14.04 (13.98). FT-IR bands (KBr, cm^{-1}): 1596 ν(HC=N); 3192, 2963 ν(H_2C-CH_2); 1626 ν(-CO); 3497 ν(-NH). ^{1}H NMR (300 MHz, $CDCl_3$) (ppm): δ 8.26 (s, 1H, HC=N); δ 6.58-7.88 (m, 8H, Ar-H); δ 2.04, 3.35 (q, q, 8H, -CH_2), δ 10.22 (s, 1H, -NH), ν 1.78 (acetone). UV-vis (DMSO, nm): 280,371. ESI-MS: Found *m/z* = 298.24 [M-H] (calcd value: *m/z* = 299).

Synthesis of Cu/Zn(II) complexes: The metal complexes were prepared by the mixing a methanolic solution of ligands and metal ions respectively in the molar radio1:2. The reaction mixtures were separately mixed and stirred at room temperature for about 1 h. Then the resulting solutions were reduced, filtered and kept aside separately for slow evaporation to dryness. The final products were washed with several times cold methanol, diethyl ether and dried *in vacuo* (**Scheme-II**).

[Cu(L1)$_2$] (1): Yield: 66 %. m.p.: 240 ºC, colour: green. Anal. calcd. (found) % for $C_{36}H_{38}N_6O_2Cu$: C, 66.49 (66.01); H, 5.89 (5.28); N, 12.92 (12.09). FTIR bands (KBr, cm^{-1}):1610 ν(C=N); 2962, 2857 ν(CH_2-CH_2); 1646 ν(-CO); 3282 ν(-NH); 399 ν(M-N); 678 ν(M-O). UV-vis (DMSO, nm): 272, 365, 573, 681. ESI-MS: Found *m/z* = 649.97 [M+H] (calcd. value: 649).

[Zn(L1)$_2$] (2): Yield: 58 %. m.p.: 222 ºC, colour: yellowish brown. Anal. calcd. (found) % for $C_{36}H_{38}N_6O_2Zn$: C, 66.30 (66.14); H, 5.87 (5.62); N, 12.89 (12.42). FTIR bands (KBr, cm^{-1}): 1614 ν(C=N); 2987, 2833 ν(CH_2-CH_2); 1633 ν(-CO); 3184 ν(-NH); 400 ν(M-N); 696 ν(M-O).UV-vis (DMSO, nm): 275,3 69. ESI-MS: Found *m/z* = 650.39 [M+H] (calcd. value: 650).

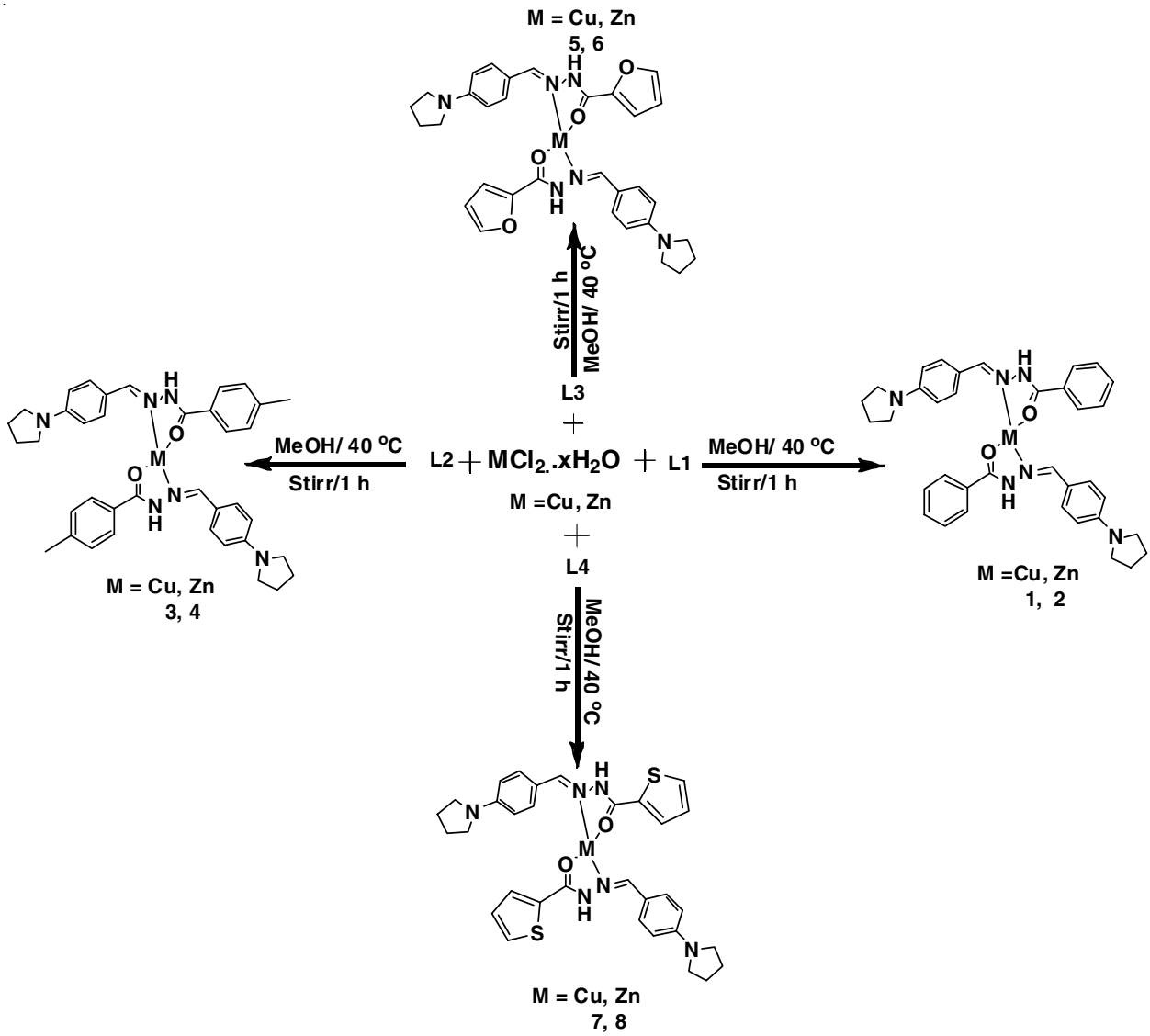

Scheme-II: Synthetic route for the preparation of Schiff base metal complexes (**1-8**)

[Cu(L2)$_2$] (3): Yield: 71 %. m.p.: 236 ºC, colour: dark green. Anal. calcd. (found) % for $C_{38}H_{42}N_6O_2Cu$ (%): C, 67.28 (67.14); H, 6.24 (6.03); N, 12. 39 (11.98). FTIR bands (KBr, cm^{-1}): 1593 ν(C=N); 2950, 2851 ν(CH$_2$-CH$_2$); 1624 ν(-CO); 3321 ν(-NH); 498 ν(M-N); 619 ν(M-O). UV-vis (DMSO, nm): 262, 350, 558, 679. ESI-MS: Found *m/z* = 675.75 [M-H] (calcd. value: 677).

[Zn(L2)$_2$] (4): Yield: 62 %. m.p.: 225 ºC, colour: brownish yellow. Anal. calcd. (found) % for $C_{38}H_{42}N_6O_2Zn$ (%): C, 67.10 (67.04); H, 6.22 (6.01); N, 12. 36 (12.11). FTIR bands (KBr, cm^{-1}): 1602 ν(C=N); 2958, 2869 ν(CH$_2$-CH$_2$); 1692 ν(-CO); 3406 ν(-NH); 522 ν(M-N); 628 ν(M-O). UV-vis (DMSO, nm): 258, 358. ESI-MS: Found *m/z* = 679.86 [M-H] (calcd. value: 680).

[Cu(L3)$_2$] (5): Yield: 72 %, m.p.: 260 ºC, colour: dark green. Anal. calcd. (found) % for $C_{32}H_{34}N_6O_4Cu$ (%): C, 60.99 (60.24); H, 5.44 (5.16); N, 13.34 (13.02). FTIR bands (KBr, cm^{-1}): 1601 ν(C=N); 2958, 2845 ν(CH$_2$-CH$_2$); 1621 ν(-CO); 3178 ν(-NH); 399 ν(M-N); 623 ν(M-O). UV-vis (DMSO, nm): 266, 363, 554, 683. ESI-MS: Found *m/z* = 631.14 [M+H] (calcd. value: 630).

[Zn(L3)$_2$] (6): Yield: 63 %, m.p.: 246 ºC, colour: brown. Anal. calcd. (found) % for $C_{32}H_{34}N_6O_4Zn$ (%): C, 60.81 (60.44); H, 5.42 (5.23); N, 13.30 (13.07). FTIR bands (KBr, cm^{-1}): 1606 ν(C=N); 2951, 2856 ν(CH$_2$-CH$_2$); 1624 ν(-CO); 3227 ν(-NH); 568 ν(M-N); 634 ν(M-O). UV-vis (DMSO, nm): 269, 366. ESI-MS: Found *m/z* = 633.25 [M+H] (calcd. value: 632).

[Cu(L4)$_2$] (7): Yield: 72 %, m.p.: 220 ºC, colour: dark green. Anal. calcd. (found) % for $C_{32}H_{34}N_6O_2S_2Cu$ (%): C, 58.03 (57.94); H, 5.17 (5.12); N, 12.69 (12.18). FTIR bands (KBr, cm^{-1}): 1585 ν(C=N); 2938, 2862 ν(CH$_2$-CH$_2$); 1603 ν(-CO); 3223 ν(-NH); 399 ν(M-N); 544 ν(M-O). UV-vis (DMSO, nm): 253, 364, 568, 677. ESI-MS: Found *m/z* = 658.18 [M-H] (calcd. value: 660).

[Zn(L4)$_2$] (8): Yield: 69 %, m.p.: 212 ºC, colour: yellowish orange. Anal. calcd. (found) % for $C_{32}H_{34}N_6O_2S_2Zn$ (%): C, 57.87 (57.64); H, 5.16 (5.11); N, 12.65 (12.18). FTIR bands (KBr, cm^{-1}): 1570 ν(C=N); 2986, 2856 ν(CH$_2$-CH$_2$); 1603 ν(-CO); 3391 ν(-NH); 401 ν(M-N); 524 ν(M-O).UV-vis (DMSO, nm): 263, 364. ESI-MS: Found *m/z* = 663.20 [M-H] (calcd. value: 664).

Solubility and stability: All the synthesized metal complexes (**1-8**) were found to be soluble completely in DMF and DMSO and stable in the solid phase at ambient temperature.

Electronic absorption spectra: The HS-DNA binding with transition metal complexes experiments was carried out by UV-visible spectroscopy titration method by using its known extinction coefficient at 260 nm (~6600 M^{-1} cm^{-1}) wavelength in an aqueous solution of tris buffer (50 mM NaCl, 5mM Tris-HCl) (pH = 7.1). Metal complexes stock solution were prepared by using 5mM tris/10 % DMSO buffer mixture and maintained at constant (pH = 7.1), further dilutions were done in the same buffer without DMSO. The intrinsic binding constants (K_b) for the interaction of these prepared transition metal complexes (**1-8**) with HS-DNA were calculated based on the electronic absor-ption spectra changes instigated by the fixed concentration of metal complexes (1×10^{-4} M) at increasing concentration of HS-DNA from 0 μM to 300 μM. The K_b values were obtained based on the following equation [30]:

$$\frac{[DNA]}{(\varepsilon_a - \varepsilon_f)} = \frac{[DNA]}{(\varepsilon_b - \varepsilon_f)} + \frac{1}{K_b(\varepsilon_b - \varepsilon_f)} \quad (1)$$

In plots of [DNA]/($\varepsilon_b - \varepsilon_f$) *vs.* [DNA], K_b is calculated from the ratio of the slope/intercept. The interaction pattern between the HS-DNA binding with complexes also were studied with ethidium bromide (EtBr) bound to be HS-DNA solution by using emission spectra. The DNA]/[EtBr] wavelength from 530 nm to 700 nm (exit 525 nm) was recorded in emission spectra and addition of metal complexes (**1-8**) fixed concentrations (1×10^{-6}) with slowly increasing from 0 μM to 200 μM at room temperature measurement as reported earlier [31].

Cyclic voltammetry: The electrochemical experiments were carried out by using the electrochemical analyzer system (Model CH-680). The prepared transition copper complexes were dissolved in DMSO/tris-buffer mixture. The control experiments were measured at a fixed concentration of copper complexes in the absence of HS-DNA. The potential and current changes through the addition of HS-DNA from 0 μM to 400 μM were examined in order to inspect the binding efficiency of copper complexes with HS-DNA.

Circular dichroism (CD) spectra: Circular dichroism spectra of HS-DNA in the presence and absence of synthesized metal complexes (**1-8**) were recorded on a spectropolarimeter JASCO J-810 from 163 nm to 900 nm by using 1 mm quartz cuvette. All the test sample solution (30 μM) was scanned in the range from 220 nm to 300 nm. Circular dichroism spectra were collected by used scan speed of 100 nm min^{-1} and one or second-time response from which the tris buffer pH = 7.1 background have been subtracted. [DNA] = 100 μM [32].

Nuclease activity: The extent of DNA cleaving efficiency of metal complexes studies were carried out by agarose gel electrophoresis method. Super-coiled pUC19 plasmid DNA was isolated from culture media. The loading dye of 1% agarose gel and tris buffer (pH = 7.1) solution were used. The prepared test samples were dissolved in blank solvent (DMSO). The metal complexes (**1-8**) (50 μM) and H_2O_2 (60 μM) test samples were added to the isolated pUC19 plasmid DNA (40 μM) and incubated at 37 ºC for 1 h in a dark chamber. After incubation, 30 μL of pUC plasmid DNA sample was mixed with a buffer solution covering 25 % bromophenol blue, 0.25 % xylene cyanol, 30 % glycerol (3 μL) and finally added on 1.0 % agarose gel containing 0.51 g mL^{-1} ethidium bromide (EtBr) as report [33].

Molecular docking studies: The molecular docking studies were executed by using Patch Dock web server. The interactive molecular graphics were used for accounting reasonable docking modes of protein, enzymes and DNA molecule [34]. Using Chem Bio Draw program, three-dimensional structure of metal complexes were portrayed and converted to PDB file format (http://www.cambridgesoft.com) online software. The 3D-molecular structure of B-DNA (PDB ID: 1-BNA, sequenced [CCGTCGACGG]2) was saved by using Protein Data Bank (http://www.rcsb.org./pdb) online software [35]. The 3D molecular structure of copper and zinc complexes were docked by uploading online server for patch docking. The 3D structure of metal

complexes visualization of molecular docked pose was accompanied by using the PyMOL molecular graphics package.

Protein binding studies: The binding interaction studies between metal complexes (**1-8**) and bovine serum albumin (BSA) have made by absorption and emission spectra measurements. BSA (stock solution) was prepared using phosphate buffer saline (PBS) pH = 7.1 and stored in the dark at 4 ºC for further use. The concentration of BSA measured at a fixed excitation wavelength at 280 nm and corresponding to BSA as emission at 345 nm, assignable to that of free BSA by molar extinction coefficient (~44,000 $dm^3 mol^{-1} cm^{-1}$) [36]. The emission excitation slit width and scan rates were continuously preserved for all experiments. The stock solution of the test samples was prepared by dissolving them in DMSO/PBS buffer pH = 7.1 and diluted suitably for required concentrations. BSA solution 2 mL (1 µM) was titrated with successive additions of a 20 µL stock solution of metal complexes (1×10^{-3} M) by using a micropipette. UV-vis absorption spectra experiments were measured BSA (10 µM) titrated with metal complexes (**1-8**) concentrations (10 µM) at room temperature.

Antibacterial activity: The *in vitro* antibacterial screening of the synthesized ligands (**L1-L4**) and its metal complexes (**1-8**) were tested separately by using the zone of inhibition (ZI) method. The human pathogens *Staphylococcus aureus*, *Staphylococcus epidermidis* (Gram-positive) and *Escherichia coli*, *Pseudomonas aeruginosa*, *Salmonella typhi* (Gram-negative) cultures were prepared and swabbed in Hinton broth containing agar plates. The prepared plates were incubated for 24 h at 37 ºC. The test DMSO solution of 10 µg/mL of metal complexes (initially dissolved in blank DMSO solvent, separately) was poured to each disc by using a micropipette and standard drug (gentamycin) (10 µg/mL disc) against Gram positive bacteria and Gram negative bacteria. Zone of inhibition was measured in 'mm' and compared with a gentamycin drug (standard).

MTT assay: The efficiency of metal complexes on the cell viability of HeLa and U937 cancer cell was determined by (3-(4,5-dimethylthiozol-2-yl)-2,5-diphenyltetrazolium bromide) MTT assay method in 96-well microplates. The cancer cells were plated at a density 1×10^5 cells/well in 200 µL of medium and incubated overnight at 37 ºC, 5 % CO_2, 95 % air and 100 % relative humidity for 24 h. The different concentration of ligands (**L1-L4**) solutions from 0 µM to 500 µM and its metal complexes from 0 µM to 50 µM in DMSO solvent was added to the monolayer. DMSO solvent was used as a control. After 24 h, the medium was replaced by fresh medium and the cultures were allowed to grow for an additional 24 h. The cell cultures were assayed subsequently by the addition of 50 µL of 5 mg mL^{-1} MTT and incubation for 4 h at 37 ºC. The extracellular medium containing MTT was removed and formazan crystals solubilized in 100 µL of DMSO. The UV-visible absorbance was measured at 570 nm using a microplate reader [37].

Morphological studies

Cell morphological analysis: Morphological changes in apoptotic cells were observed by scanning electron microscopy (SEM). HeLa cells were seeded in a heat-sterilized coverslip six-well plate at 24 h, cells were exposed to Cu/Zn thiophene complexes (**7,8**) IC_{50} value concentration (40 µM) and incubated for 24 h. HeLa cells were fixed in 2.5 % glutaraldehyde in 0.075 M PBS buffer solution condition for 1 h and one or three times washed with cells in PBS buffer medium. Cells were fixed in 0.25 % aqueous osmium tetroxide added (30 min). After cells were washed one or three times in distilled water in a fume cupboard. The test samples were dehydrated with various concentrations of ethanol (30, 50, 70, 80, 90, 95 and 100 %) in time intervals of 10 min for 1 h. Finally, 100 % of ethanol was added in a desiccator overnight to dry the sample.

RESULTS AND DISCUSSION

^{1}H NMR spectra: The ^{1}H NMR spectra of ligands (**L1-L4**) show a single peak at δ 8.25 ppm (L1), δ 8.27 ppm (L2), δ 8.06 ppm (L3) and δ 8.26 ppm (L4) (-HC=N-) protons observed for the azomethine group. This peak provides a piece of strong evidence for the Schiff base formation. The ligands (**L1-L4**) show a single peak appearing at δ 9.37 ppm, δ 10.86 ppm, δ 9.21 ppm and δ 10.22 ppm may be ascribed to >NH groups. A bunch of peaks due to aromatic, furan and thiophene protons appear in the range from δ 6.54 to 7.88 ppm in hydrazone ligands (**L1-L4**). The presence of pyrrolidine ring (N-substituted heterocyclic ring) contains two types of protons peak appeared form δ 1.64 to 3.75 ppm were attributed to the CH_2 protons. The appearance of a sharp single peak at δ 2.41 ppm in L2 is due to aromatic ring substituted CH3 proton.

On a similar basis, ^{1}H NMR spectra of [Zn(L1-L4)$_2$] complexes were recorded in DMSO-d_6 solution. The imine proton signal observed at δ 8.28 ppm (L1), δ 8.24 ppm (L2), δ 8.27 ppm (L3) and δ 8.25 ppm (L4) splits into the single sharp peak azomethine protons shifted to downfield region assigned as zinc complexes formation, which indicates the participation of azomethine group in coordination with metal. The downfield region shift of >NH protons in all zinc complexes proposes the coordination of >C=O to the metal ions. The >NH groups of a single peak may be assigned and appreciable downfield shifted to δ 11.54 ppm (2), δ 11.51 ppm (4), δ 11.46 ppm (6) and δ 11.54 ppm (8) show zinc complexes. A number of signals peak observed in ligands around from 6.20 to 7.88 ppm are assigned to the aromatic, furan and thiophene ring protons and show minor shifts in its zinc complexes [38]. Another feature is the pyrrolidine ring peak was small shifted to 1.94-3.62 ppm zinc complexes appeared aliphatic CH_2 protons. The downfield of imine protons in the zinc complexes formation as compared to the Schiff base ligand, suggests the coordination of the azomethine (-HC=N-) group and carbonyl group (>C=O) interact to the metal ion.

^{13}C NMR spectrum provides additional values for the direct information about the ligands (**L1-L4**). The carbon peaks show around at δ 153.91 ppm (**L1**), δ 154.45 ppm (**L2**), δ 150.18 ppm (**L3**) and δ 149.23 ppm (**L4**) may be the appearance of azomethine (HC=N-) carbon. The ligands show a cluster of carbons peaks between 111.58 to 158.44 ppm, respectively, corresponding to phenyl ring, furan and thiophene carbons. The carbonyl carbon signals at from (HC=N-) δ 161 ppm to (HC=N-) δ 179 ppm, are attributed to HN-C=O carbons present in the NMR spectra, respectively. The pyrrolidine ring (N-substituted heterocyclic carbon) peak around at from δ 25.48 ppm to 52.64 ppm upfield regions were due to CH_2 carbon atom presented in ligands. The L2 ligand show methyl carbon peak at δ 11.99

ppm, which confirms the methyl carbon attached the aromatic phenyl ring.

IR spectra: The IR spectra experiments were carried out to provide valuable information about the coordination sites of the hydrazone moiety of Schiff base ligands. On comparing the spectral results of ligands and their metal complexes, the presence of ν(C=N) bands at 1626 cm^{-1} (L1), 1607 cm^{-1} (L2), 1592 cm^{-1} (L3) and 1596 cm^{-1} (L4) assigned to azomethine nitrogen stretching vibrations of ligands and the bands at 1610 cm^{-1} (1), 1603 cm^{-1} (2), 1590 cm^{-1} (3), 1592 cm^{-1} (4), 1589 cm^{-1} (5), 1590 cm^{-1} (6), 1585 cm^{-1} (7), 1570 cm^{-1} (8) assigned to azomethine nitrogen coordination in the copper and zinc metal ion clearly indicate the formation of metal complexes. Further, the absorption bands due to ν(C=O) stretching groups of the ligands and complexes at 1632 cm^{-1} (L1), 1637 cm^{-1} (L2), 1646 cm^{-1} (L3), 1628 cm^{-1} (L4) and complexes formation at 1621 cm^{-1} (**1**), 1629 cm^{-1} (**2**), 1614 cm^{-1} (**3**), 1631 cm^{-1} (**4**), 1623 cm^{-1} (**5**),1639 cm^{-1} (**6**), 1609 cm^{-1} (**7**), 1611 cm^{-1} (**8**), respectively also confirm the carbonyl coordination to the central metal ion. Both N, O coordination bands shifts from 2 to 17 cm^{-1} confirm donation of lone pair electron present in the azomethine nitrogen, carbonyl oxygen to the metal ion [39]. The IR spectral band due to (NH) not showed any significant band shift indicate non-participation of amide group in coordination processes [40]. The presence of new bands in the region from 522-399 cm^{-1} and 678-524 cm^{-1} in the metal complexes (**1-8**) may be assigned to ν(M-N) and ν(M-O) complexes, respectively [41]. Finally, IR spectra data suggest NO bidentate behaviour of the hydrazone ligands.

Mass spectra: The ESI-mass spectra of ligands (**L1-L4**) and their metal complexes (**1-8**) were recorded in methanol. The mass spectra of the isolated ligands show the molecular ion peaks value observed at *m/z* 294.30 (L1), 306.10 (L2), 283.08 (L3), 298.24 (L4) [M ± H] equivalents to their molecular weight for the Schiff base ligands. Molecular ion peaks of complexes exhibits at *m/z* = 649.97 (**1**), 650.39 (**2**), 675.75 (**3**), 679.86 (**4**), 631.14 (**5**), 633.25 (**6**), 658.18 (**7**) and 663.20 (**8**) [M ± H], respectively, which have evidently support the composition of the Schiff base complexes.

Electronic spectra: UV-visible spectroscopy studies of hydrazone ligands (**L1-L4**) and its metal complexes (**1-8**) were recorded in DMSO solution from 200 nm to 800 nm at room temperature. The absorption bands in the region of 253-283 nm and 363-365 nm of metal complexes are due to the π-π* and n-π* transitions associated with phenyl ring, imine chromophore and carbonyl group of the coordinated metal complexes [42]. The spectra of the complexes were slightly shifted to 2-10 nm (wavelength), the result of the enlargement of the conjugate structure shows the coordination of metal ions with ligands [43]. The broad bands at approximately 554-573 nm are attributed to the ligand to metal charge transfer (LMCT) transitions, which may be due to the overlapping of the LMCT transitions of O → M and N → M. The weak *d-d* bands due to the transition $^2B_{1g} \rightarrow {}^2A_{1g}$ and $^2B_{1g} \rightarrow {}^2E_g$ at 676-684 nm, visible region suggesting square planar geometry for copper complexes [44]. However, zinc complexes not show *d-d* electronic transitions, due to d^{10} orbital and its diamagnetic nature [45]. The empirical formula, elemental and mass spectral data assigned the tetrahedral geometry for zinc complexes [46].

Electrochemical studies: Electrochemical properties of copper complexes were recorded in DMSO solution in the potential range from -0.2 V to + 0.4 V and at a scan rate of 50 mV s^{-1}. Ag/AgCl-reference electrode and TBAP supporting electrolyte were used. The redox peaks emerge at 0.018- 0.041 V are attributed to the cathodic peaks and 0.107-0.141 V anodic peaks, corresponding to the transfer of Cu(II)/Cu(I) and Cu(I)/Cu(II) are summarized in Table-1, confirming copper complexes are redox active and quasi-reversible one electron transfer reduction process [47,48].

TABLE-1
CYCLIC VOLTAMMERTRIC BEHAVIOUR OF ALL COPPER COMPLEXES IN (V)

Complexes	E_{pa}	E_{pc}	$*\Delta E_p$	$*E_{1/2}$	i_{pa}/i_{pc}
$[Cu(L1)_2]$ (1)	0.122	0.018	0.104	0.070	1.17
$[Cu(L2)_2]$ (3)	0.141	0.026	0.115	0.084	0.96
$[Cu(L3)_2]$ (5)	0.112	0.028	0.084	0.070	0.94
$[Cu(L4)_2]$ (7)	0.107	0.041	0.066	0.074	0.60

$*\Delta E_p = E_{pa} - E_{pc}$; $*E_{1/2} = E_{pa} + E_{pc}/2$

DNA binding studies

Electronic spectroscopy: The DNA binding interaction with metal complexes (**1-8**) was demonstrated by using electronic absorption titration method, in the concentration range of HS-DNA from 0 μM to 100 μM at a fixed concentration of metal complexes (300 μM) and in the spectral range of 200-500 nm. The obtained electronic spectra are given in Fig. 1. The high energy absorption bands have appeared in the spectra of respective metal complexes below 300 nm, which may be attributed to intense π-π* intra-ligand charge transfer transitions and the bands around 360-380 nm are due to the ligand to metal charge transfer (LMCT). The absorption bands of metal complexes with the addition of DNA showed changes in spectra and significant hypsochromic shifts, complemented with a redshift. The HS-DNA stabilization may be attributed to slight stacking interaction between the aromatic chromophores of the base pairs DNA [49]. The UV-visible experimental results are inconsistent with the interacalative binding mode. In order to quantify the binding strength of the copper and zinc complexes are summarized in Table-2, the binding constant (K_b) was calculated and found to be in the order of: **7 > 8 > 5 > 6 > 3 > 4 > 1 > 2**.

Emission spectroscopy: The quenching experiments can provide essential information on HS-DNA binding ability. Steady-state competitive binding experiments between ethidium bromide (sensitive fluorescence probe) and metal complexes (quenchers) for HS-DNA in tris buffer (pH = 7.1) were carried out. The titration spectra of the EB-DNA system in presence and absence of metal complexes (**1-8**) is observed in Fig. 2. No emission was observed for both metal complexes and DNA in control experiments. The molecular fluorophore (EtBr) emits at 603 nm in the presence of HS-DNA due to strong stacking interaction between the adjacent base pairs of DNA. The significant shift (red) in titration quenching spectra with an increase in the concentration of the metal complexes, clearly indicating that EB molecules are depicted in Fig. 3 by metal complexes from their HS-DNA binding sites and its better understanding with the linear Stern-Volmer equation [50].

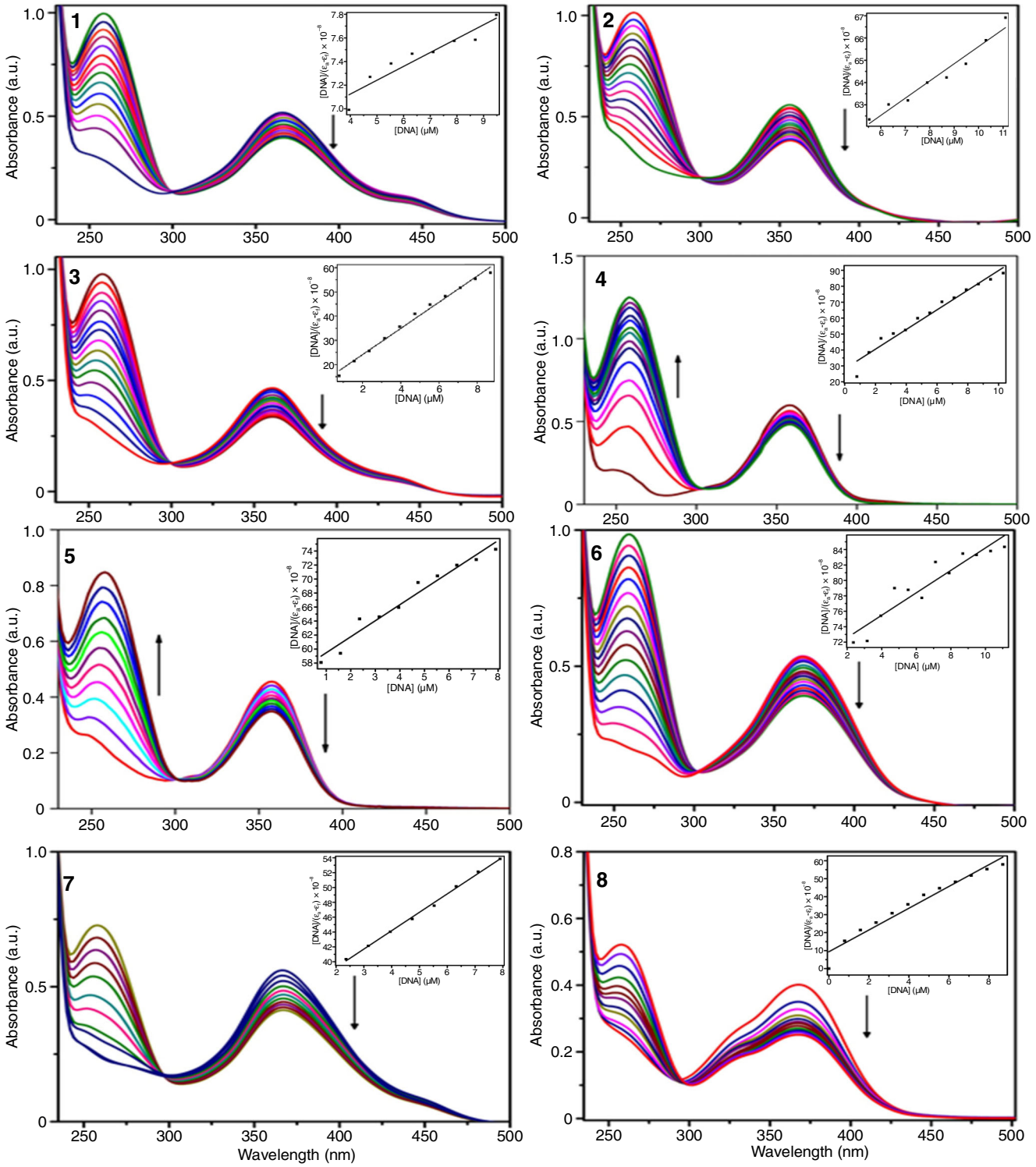

Fig. 1. Absorption spectra of metal complexes (**1-8**) in the absence and presence of increasing amounts of HS-DNA for tris buffer (pH = 7.1). The arrow shows that the changes in absorbance with respect to increasing in the HS-DNA concentration. Inset: Plot between [DNA] and [DNA]/($\varepsilon_a - \varepsilon_f$)

$$I_o/I = K_{sv}\,[Q] + 1 \quad (2)$$

K_{sv} values found in the slope and intercept of the plot I_o/I *versus* [Q] are exhibited in Table-3 for metal complexes. The spectral data reveals that DNA-bound EB can be more readily replaced in these following order: **7 > 8 > 5 > 6 > 3 > 4 > 1 > 2**,which is consistent with the results obtained in the electronic absorption spectral studies.

Further, the DNA apparent binding constant (K_{app}) values obtained for the metal complexes were also calculated using the following equation:

$$K_{EtBr}\,[EtBr] = K_{app}\,[complex]_{50} \quad (3)$$

where K_{EtBr} equals 1.0×10^7 M^{-1} is the DNA binding constant of EtBr, [EtBr] is the concentration of (10 μM) and $[complex]_{50}$ is the various concentration of the metal complexes (**1-8**) that

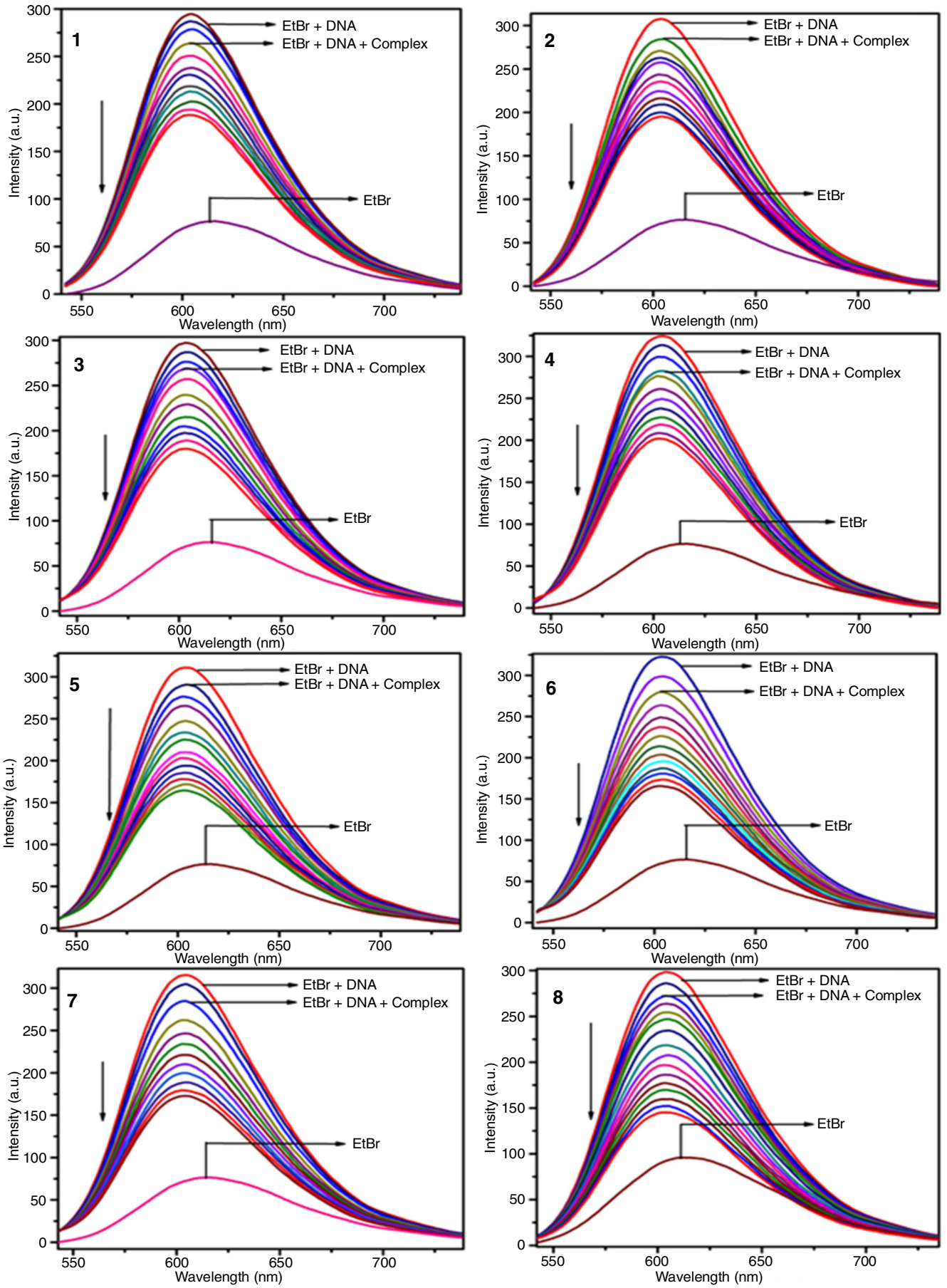

Fig. 2. Emission spectra of EtBr bound to HS–DNA(10 μM) in the presence of (0–200 μM) concentration metal complexes (**1-8**) in Tris–HCl buffer pH = 7.1. Arrow indicates the changes in the emission intensity as a function of metal complexes concentration

TABLE-2
ELECTROCHEMICAL BEHAVIOUR OF COPPER COMPLEXES IN TRIS BUFFER (pH = 7.1) IN THE ABSENCE AND PRESENCE OF HS-DNA IN (V)

Complexes	R	E_{pa}	E_{pc}	ΔE_p	$E_{1/2}$	i_{pa}/i_{pc}
$[Cu(L1)_2]$ (1)	0	0.059	-0.023	0.082	0.0180	0.930
	0.100	0.063	-0.002	0.065	0.0310	0.990
	0.200	0.065	0.010	0.055	0.0360	1.050
$[Cu(L2)_2]$ (3)	0	0.035	-0.064	0.099	-0.0150	0.830
	0.100	0.064	-0.079	0.143	-0.0076	0.730
	0.200	0.070	-0.075	0.145	-0.0050	0.820
	0.300	0.072	-0.075	0.147	-0.0015	0.790
$[Cu(L3)_2]$ (5)	0	0.039	-0.040	0.079	-0.0010	0.790
	0.100	0.067	-0.071	0.138	-0.0020	0.720
	0.200	0.065	-0.054	0.119	0.0060	0.804
	0.300	0.062	-0.039	0.101	0.0120	0.860
$[Cu(L4)_2]$ (7)	0	0.057	-0.033	0.090	0.0120	0.980
	0.100	0.066	-0.023	0.089	0.0220	0.923
	0.200	0.065	-0.019	0.084	0.0230	0.880
	0.300	0.063	-0.015	0.078	0.0240	0.880

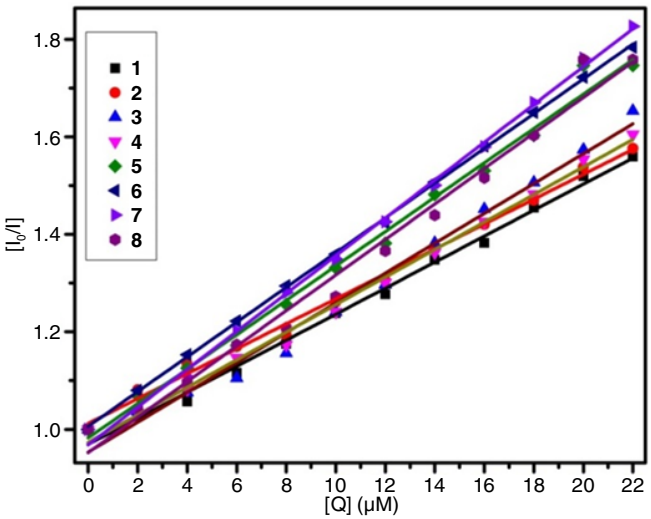

Fig. 3. Stern-Volmer plots of the emission titrations of metal complexes (**1-8**)

TABLE-3
ABSORPTION BINDING CONSTANT (K_b), EMISSION QUENCHING CONSTANT (K_{sv}) AND APPARENT BINDING CONSTANT (K_{app}) BETWEEN HS-DNA AND METAL COMPLEXES (**1-8**)

Complexes	H (%)	K_b (M^{-1}) 1×10^3	K_{sv} (M^{-1}) 1×10^5	K_{app}(M^{-1}) 1×10^6
$[Cu(L1)_2]$ (1)	24.04	1.76	2.76	0.76
$[Zn(L1)_2]$ (2)	31.96	1.33	2.53	0.66
$[Cu(L2)_2]$ (3)	27.89	2.19	3.21	0.82
$[Zn(L2)_2]$ (4)	19.39	2.09	2.90	0.63
$[Cu(L3)_2]$ (5)	19.64	4.01	3.59	0.71
$[Zn(L3)_2]$ (6)	27.41	2.29	3.54	0.69
$[Cu(L4)_2]$ (7)	26.38	7.24	4.01	0.90
$[Zn(L4)_2]$ (8)	33.29	6.48	3.83	0.74

causes 50 % reduction in the emission intensity of DNA pretreated with EtBr. These K_{app} values are summarized in Table-3 reflect by the ability of metal complexes to replace EtBr from [EtBr+DNA] complexes through interaction between intercalation mode. Both intrinsic binding constant and apparent binding constant value clearly indicate that all the copper and zinc complexes have a good interaction binding affinity towards HS-DNA. Thiophene complexes (**7**,**8**) displaced EtBr efficiently than the other **1-6** complexes, the higher K_{sv} experiential values show for thiophene complexes (**7**,**8**) designate the strong strength binding affinity towards HS-DNA. The K_{app} values for the metal complexes order to **7 > 3 > 1 > 8 > 5 > 6 > 2 > 4** indicates that metal complexes interaction with HS-DNA nucleotides.

Electrochemical titrations: Cyclic voltammetry experiments were performed for all the Cu(II) complexes in the absence and presence of incremental addition of HS-DNA in tris buffer/DMSO mixture solution at a scan rate of 50 mV s^{-1}. The instruments show the absence of HS-DNA, non-Nernstian performance with a one-electron Cu(II)/Cu(I) redox process and quasi-reversible [51] with peak potential separation of -11 mV to 245 mV were observed. On titration with DNA, a negligible potential shift in the cathodic peak and anodic peak along with the repression of both peak currents as expected, demonstrating the intercalation modes by Cu-chelates (Fig. 4) [52].

Circular dichroism (CD) studies: The CD spectral technique was considered as a valuable, powerful and sensitive identify DNA morphology during a DNA-drug interaction [53]. In the CD spectra were measured as an HS-DNA shows a positive band at 275 nm due to base stacking and the negative band near 245 nm arises from the right-handed helicity of β-DNA, respectively [54]. The intercalation binding mode which may enhance the intensity of both the above bands and thus stabilizing the right-hand β conformation of DNA [55]. The CD spectra of HS-DNA in the absence and presence of the metal complexes (**1-8**) show an increase in the ellipticity of both the positive bands and slightly shift (red) to (1-3 nm) in [ML]/[DNA], are depicted in Fig. 5. The negative bands nearly 1-4 nm red shift followed by the ratio of [ML]/[DNA] indicating the metal complexes having an effect on the helicity structure of DNA. The spectra ellipticity changes metal complexes are in good interaction with their HS-DNA binding ability and conformation of intercalative binding mode. The CD results are found consistent with those of UV-vis absorption and emission spectra.

DNA cleavage activity: The extent nuclease activity of the efficient metal complexes (**1-8**) was investigated for supercoiled pUC 19 plasmid DNA (40 μM in base pairs) using gel electrophoresis technique. In control, either metal complexes

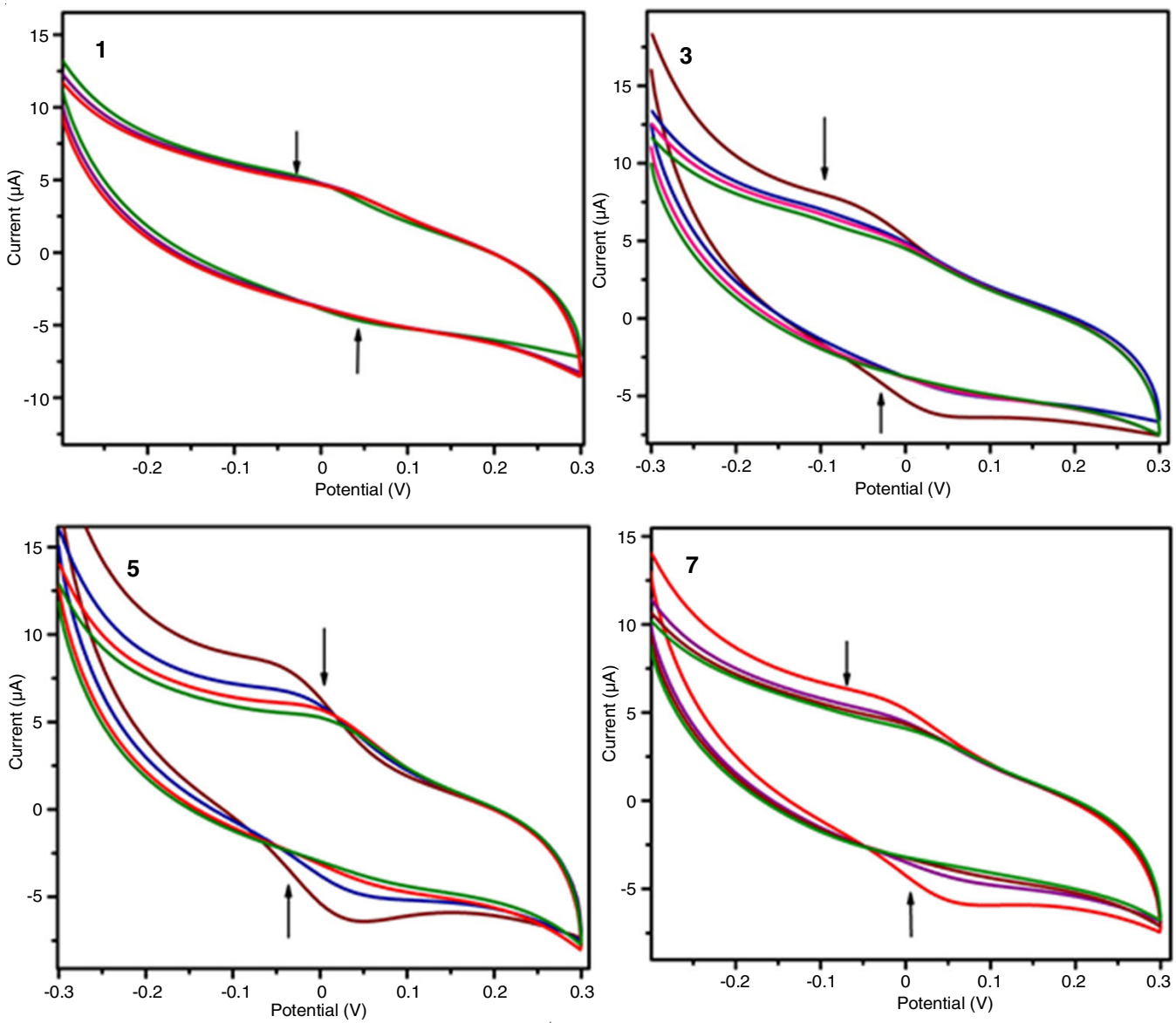

Fig. 4. Cyclic voltammograms of all copper complexes [1 × 10^{-4} M] in the absence and presence of HS-DNA in Tris–HCl buffer = pH 7.1/ DMSO mixture solution at a scan rate of 50 mV s^{-1}. The arrow indicates upon the increasing amount of HS-DNA

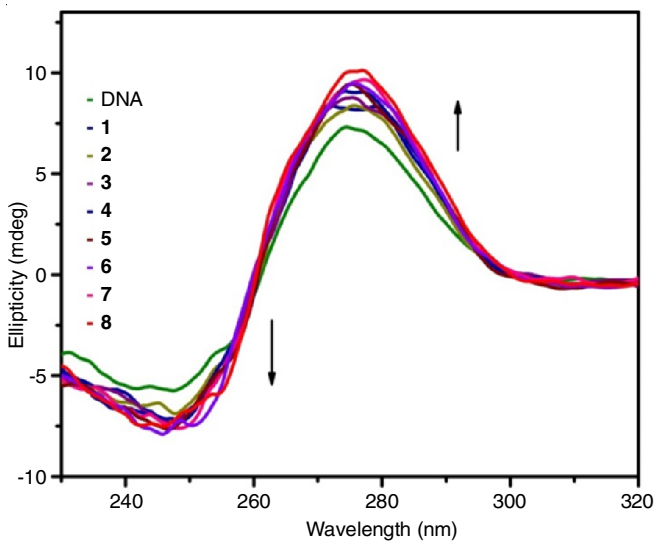

Fig. 5. Circular dichroism spectra of HS–DNA (100 μM) in the absence and presence of metal complexes (**1-8**) (30 μM) in Tris–HCl buffer pH = 7.1 at room temperature

or H_2O_2 do not exhibit DNA cleavage under experimental conditions. But metal complexes shows DNA cleavage efficiently in the presence H_2O_2 (60 μM) *via* formation of reduced metal ions and hydroxyl radical which enable them to cleave DNA by Fenton mechanism [56,57]. This was observed in the gel electrophoresis by monitoring the transfer of naturally occurring covalently closed circular form (form I) to the open circular relaxed form (II) as depicted in Fig. 6. The experimental results for nuclease activity of metal complexes have the same strength to cleave the pUC19 plasmid DNA with H_2O_2.

Molecular docking studies: Molecular docking studies has an important role in perceptual of drug-DNA interaction for selective new chemotherapeutic drugs design and the technique has confirmed the efficiency of binding ability understating the binding mechanism of the small molecule to DNA [58]. The patch molecular docking studies have been executed β-DNA (PDB ID: 1BNA) in the presence of metal complexes (**1-8**) with DNA duplex of sequenced (CGCGAATTCGCG)2 in order to preliminarily determine the specific binding site

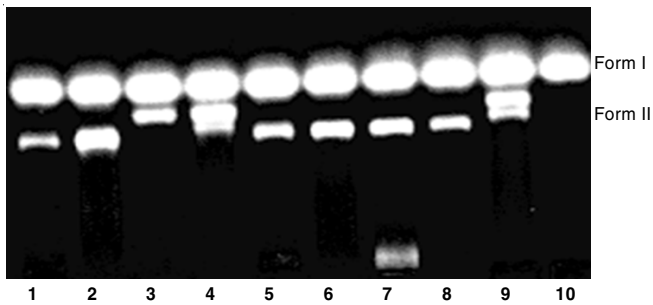

Fig. 6. Gel electrophoresis showing the chemical nuclease activity of the supercoiled pUC19 DNA (40 μM) incubated at 37 °C for 1 h in Tris–HCl buffer pH = 7.1 with fixed concentration of metal complexes (**1-8**) (50 μM) in the presence H_2O_2 as an oxidizing agent (60 μM): Lane: 10. DNA alone, lane: 9. DNA + H_2O_2, lane: 1. DNA + H_2O_2 + **1**, lane: 2. DNA + H_2O_2 + **2**, lane: 3. DNA + H_2O_2 + **3**, lane: 4. DNA + H_2O_2 + **4**, lane: 5. DNA + H_2O_2 + **5**, lane: 6. DNA + H_2O_2 + **6**, lane: 7. DNA + H_2O_2 + **7**, lane: 8. DNA + H_2O_2 + **8**

alongside with the chosen alignment of sterically adequate metal complexes inside the DNA. It has been identified that the metal complexes interact through the intercalative binding mode to DNA and become a stable, hydrogen bonding, energy and hydrophobic interactions with DNA [59], which can define the stability in the intercalative binding mode metal complexes with DNA is observed (Table-4). The docking results display the metal complexes binding efficiency with the DNA receptor and reveal binding affinity order to **7** > **8** > **5** > **6** > **3** > **4** > **1** > **2**, respectively. The molecular docking negative energy values recommend an effective binding affinity. In particular, thiophene Cu/Zn(II) complexes (**7**, **8**) have relatively more negative values with effective binding energy and improving the strong DNA binding affinity than the other metal complexes (**1-6**).

Protein binding studies

Electronic absorption titration spectral studies: Electronic absorption spectroscopic analyses were performed to understands the changes of BSA in the presence of metal complexes (**1-8**). UV-Vis spectra showed the intensity of BSA at 280 nm were enhanced upon the addition of complexes (**1-8**), suggesting static interaction due to the formation of the ground state complexes with BSA as reported earlier [60].

Fluorescence quenching studies of BSA: The fluorescence spectroscopic experiment is carried out the interactions between metal complexes (**1-8**) and proteins. The interaction of BSA/metal complexes are studied by using fluorescence spectra measurement at ordinary temperature (37 ºC). Bovine serum albumin is excited at λ_{ext} 280 nm and strong fluorescence peaks are observed at λ_{emi} 335 nm [61]. However, no emission peak observed around at λ_{emi} 335 nm when the metal complexes were excited with the same excitation wavelength, proposing that the metal complexes would not induce fluorescence intensity interference to albumin within the inspected excitation wavelength range. BSA solution (1×10^{-6}) is titrated with the increasing concentrations of metal complexes (0-200 μM) by quenching manner in the range from 250 to 550 nm. The addition of respective titration metal complexes/BSA interaction resulted in a substantial decrease in the intrinsic emission intensity of 335 nm along with a slight hypochromic shift of 1-15 nm for metal complexes. Finally, the results reveal that the quenching may be due to strong interactions between all metal complexes with BSA. The quenching constant (K_q) value was calculated by using the Stern-Volmer equation as shown in Fig. 7. From the plot of I_o/I *versus* [Q] and K_q value can be considered for metal complexes.

The calculated values of quenching constant (K_q) for the test compounds exhibit strong protein binding ability. The strong binding ability of the metal complexes to BSA occurs with an equilibrium binding constant and can be evaluated and represented by the Scatchard equation.

$$\log [(F_o\text{-}F)/F] = \text{Log } K_b + n \log [Q] \quad (4)$$

where K_b is the binding constant of metal complex/BSA and n is the number of binding sites. A plot of log [(F_o-F)/F] *versus* log [Q] can be used to determine both K_b and n such calculated values for metal complexes are depicted in Table-5. A n value of shows the existence of a single binding site in BSA for the metal complexes. The higher K_q and K_b values indicating a strong interaction between the BSA and metal complexes used in this study.

TABLE-5
PROTEIN BINDING CONSTANT (K_a), QUENCHING CONSTANT (K_b) AND THE NUMBER OF BINDING SITES (n) FOR METAL COMPLEXES (**1-8**)

Complexes	K_q (M^{-1}) 1×10^4	K_b (M^{-1}) 1×10^5	n
[Cu(L1)$_2$] (1)	0.8	2.08	1.45
[Zn(L1)$_2$] (2)	0.7	2.14	1.86
[Cu(L2)$_2$] (3)	1.8	2.09	2.10
[Zn(L2)$_2$] (4)	1.1	2.06	1.50
[Cu(L3)$_2$] (5)	2.1	2.10	2.04
[Zn(L3)$_2$] (6)	1.3	2.11	2.70
[Cu(L4)$_2$] (7)	3.5	2.15	2.52
[Zn(L4)$_2$] (8)	2.2	2.12	2.31

The emission spectra clearly displayed the BSA binding strength ability of the metal complexes following in the order **7** > **8** > **5** > **6** > **3** > **4** > **1** > **2**, which are consistent with in the results found from the above affinity studies.

TABLE-4
CALCULATED VALUE OF DOCKING OF β-DNA WITH METAL COMPLEXES (**1-8**)

Compound	Score	Area	ACE	Transformation
[Cu(L1)$_2$] (1)	4530	687.70	-684.10	-3.02, 0.52, -0.32, 14.04, 18.05, 24.00
[Zn(L1)$_2$] (2)	5322	811.30	-649.37	-2.96, 0.56, 0.02, 18.47, 24.08, -1.56
[Cu(L2)$_2$] (3)	4388	767.40	-761.19	-2.94, 0.82, -0.10, 19.22, 21.74, -3.09
[Zn(L2)$_2$] (4)	5040	794.40	-652.27	-1.45, 0.02, 2.82, 18.92, 24.88, 0.95
[Cu(L3)$_2$] (5)	3638	669.40	-692.02	1.25-6.06, 3.00, 13.85, 18.39, 23.77
[Zn(L3)$_2$] (6)	4178	687.70	-658.00	-1.18, -0.62, 2.17, 19.46, 20.84, -4.61
[Cu(L4)$_2$] (7)	3466	680.00	-777.68	-0.22, 0.93, 0.12, 17.44, 22.32, -4.16
[Zn(L4)$_2$] (8)	4760	733.10	-749.88	1.50, 0.76, -1.15, 19.83, 21.02, -4.87

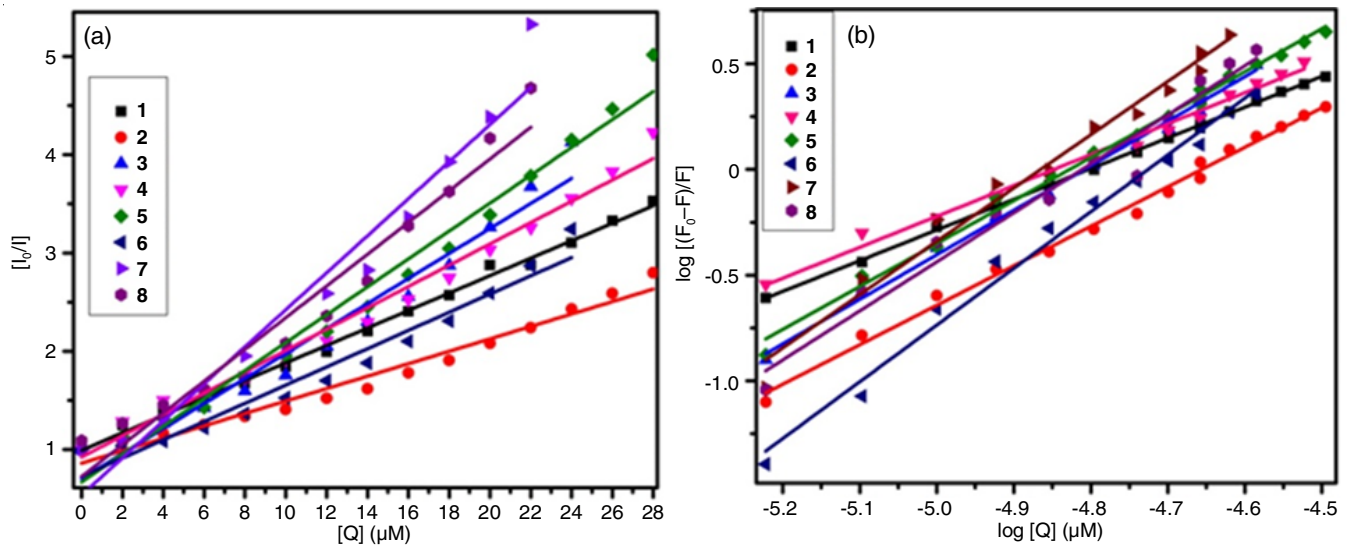

Fig. 7. Stern-Volmer plots (a), Scatchard plots (b) of the emission titrations of metal complexes (**1-8**) interaction with BSA

Biological activities

Antibacterial activity evaluation: The antibacterial activity of synthesized ligands (**L1-L4**) and their metal complexes (**1-8**) was analyzed. The zone of inhibition (mm) is used to analyze the antibacterial activity of the ligands and their metal complexes compare to standard drug. The ligands and their metal complexes showed enhance antibacterial activity against Gram-positive bacteria (*S. aureus*, *S. epidermidis*) and Gram-negative bacteria (*E. coli*, *S. typhi* and *P. aeruginosa*) compared to hydrazone ligands and standard drug. However, ligands are shown less activity than the standard drug against the same microorganism under identical experimental condition. All the copper complexes exhibited higher antibacterial activity against all bacterial species compared to all zinc complexes, which may be recognized to the atomic radius and the electronegativity of Cu(II) ion. The improved antibacterial activity of metal complexes can be explained based on Overtone's concept and chelation theory [62,63].

***in vitro* Cytotoxicity evaluation:** The efficiency of the ligands (**L1-L4**) and their metal complexes (**1-8**) in suppressing cell growth and promoting apoptosis have been studied by MTT reduction. The ability of the ligands and metal complexes to cleave the DNA molecule encouraged us to study its effect on the growth of the cancer cell line. Cytotoxicity of these ligands and metal complexes are tested against a panel of two cell lines HeLa (cervical cancer) and U937 cancer cells, and the loss of viability was determined using MTT assay [64]. The ligands (**L1-L4**) and their metal complexes (**1-8**) dissolved in DMSO and cancer cells are treated with different concentrations of the ligands and their metal complexes for 24 h. A blank sample contains the same volume of DMSO solvent. The results are analyzed by measuring the means of cell viability in Table-6. The inhibitory concentration (IC_{50}) values for the ligands and their metal complexes shows inhibition of cancer cells due to the metal complex species rather than the separated ligands, in the tested HeLa and U937 cell lines are in the order of **7 > 8 > 5 > 6 > 3 > 4 > 1 > 2 > L**. All metal complexes (**1-8**) exhibited appreciable cytotoxic effects on HeLa and U937 cell lines.

TABLE-6
in vitro CYTOTOXICITY ASSAY FOR LIGANDS (**L1-L4**) AND ITS METAL COMPLEXES (**1-8**) IN TWO DIFFERENT CELL LINES (24 h)

Compounds	IC_{50} (μM)	
	HeLa cell	U937 cell
L1	> 200	> 200
L2	> 200	> 200
L3	> 200	> 200
L4	> 200	> 200
[Cu(L1)$_2$] (1)	44.880	49.380
[Zn(L1)$_2$] (2)	48.296	53.910
[Cu(L2)$_2$] (3)	39.750	42.420
[Zn(L2)$_2$] (4)	43.820	46.790
[Cu(L3)$_2$] (5)	37.660	40.460
[Zn(L3)$_2$] (6)	44.530	45.294
[Cu(L4)$_2$] (7)	34.870	36.804
[Zn(L4)$_2$] (8)	43.316	42.209

Morphological assessment study: The morphological changes of the cell surface due to the interference of thiophene copper and zinc complexes (**7**,**8**) with HeLa cells have been displayed by means of scanning electron microscope for the untreated and treated cells as given in Fig. 8. Cells proliferated in growth medium and vehicle-treated cells were confluent without signs of distress. HeLa cells exposed to thiophene complexes (**7**,**8**) are added to the low concentration of 30 μM treated cancer cells and showed a diminished cell thickness, adjusted cells and apoptotic body size in SEM surface (10 μM) for HeLa cancer cell.

Conclusion

The present study focused on the synthesis and characterization using structural, spectral and analytical methods of bivalent hydrazone based Cu/Zn(II) complexes. The metal complexes is binded to HS-DNA, which was conformed through absorption, emission, circular dichromism and electrochemical techniques. This indicated that metal complexes (**1-8**) effectively bind with HS-DNA through intercalative binding mode between them. The gel electrophoresis method confirms the higher ability of metal complexes to cleave pUC19 plasmid DNA. The fluore-

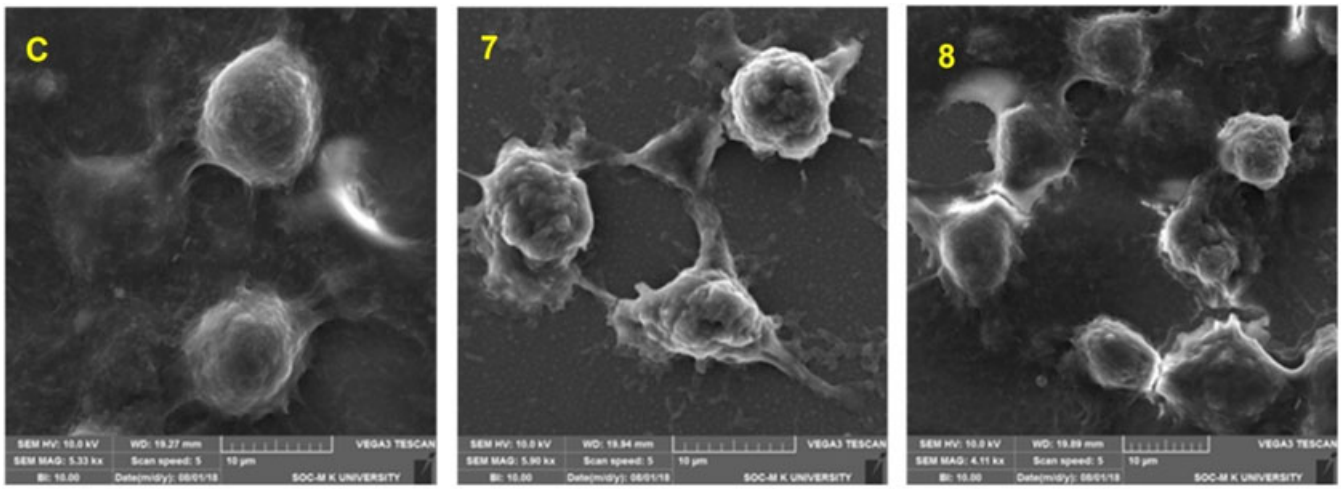

Fig. 8. Scanning electron microscopy images of thiophene Cu/Zn(II) complexes (**7, 8**) induced cell surface morphological changes and decreased cell density in the HeLa cancer cell line

scence intensity of the BSA is quenched and the quenching occurs *via* a static mode and indicates that the metal complexes bind to BSA. Further, studies showed the higher antibacterial activity of metal complexes is comparable to ligands and standard drug. The synthesized hydrazone ligands and their metal complexes were screened for cytotoxic activity against HeLa and U937 cancer cell lines and they exhibited excellent inhibitory activity to a cancer cell. The results show that the hydrazone ligands (**L1-L4**) and their metal complexes (**1-8**) are significant and deliver usage for therapeutic application.

ACKNOWLEDGEMENTS

The authors express their sincere thanks to UGC (Non-Net fellowship) for financial support. The authors are grateful to Prof. Dr. G.S. Selvam, Professor & Head, School of Biological Sciences and Dr. B. Ashok Kumar, Assoc. Prof., School of Biotechnology, Madurai Kamaraj University, for their help and providing gel electrophoresis measurements and cancer cell activity facilities. Also express their gratitude to School of Chemistry, Madurai Kamaraj University for recording FT-IR, NMR, ESI-Mass, CD spectra and SEM analyses.

CONFLICT OF INTEREST

The authors declare that there is no conflict of interests regarding the publication of this article.

REFERENCES

1. K.L. Haas and K.J. Franz, *Chem. Rev.*, **109**, 4921 (2010); https://doi.org/10.1021/cr900134a.
2. N. Arshad, P. Ali Channar, A. Saeed, S.I. Farooqi, A. Javeed, F. Ali Larik, W. Ahmad Abbasi and U. Flörke, *J. Saudi Chem. Soc.*, **22**, 1003 (2018); https://doi.org/10.1016/j.jscs.2018.05.002.
3. P. Subbaraj, A. Ramu, N. Raman and J. Dharmaraja, *J. Coord. Chem.*, **67**, 2747 (2014); https://doi.org/10.1080/00958972.2014.950256.
4. L.H. Abdel-Rahman, R.M. El-Khatib, L.A.E. Nassr and A.M. Abu-Dief, *Arab. J. Chem.*, **10**, S1835 (2017); https://doi.org/10.1016/j.arabjc.2013.07.010.
5. L.H. Abdel-Rahman, A.M. Abu-Dief, E.F. Newair and S.K. Hamdan, *J. Photochem. Photobiol. B*, **160**, 18 (2016); https://doi.org/10.1016/j.jphotobiol.2016.03.040.
6. R.F. Brissos, A. Caubet and P. Gamez, *Eur. J. Inorg. Chem.*, 2633 (2015); https://doi.org/10.1002/ejic.201500175.
7. R. Gomathi, A. Ramu and A. Murugan, *Bioinorg. Chem. Appl.*, **2014**, Article ID 215392 (2014); https://doi.org/10.1155/2014/215392.
8. A.S. Abu Surrah and M. Kettunen, *Curr. Med. Chem.*, **13**, 1337 (2006); https://doi.org/10.2174/092986706776872970.
9. M. Mohamed Subarkhan, R.N. Prabhu, R. Raj Kumar and R. Ramesh, *RSC Advances*, **6**, 25082 (2016); https://doi.org/10.1039/C5RA26071J.
10. W.H. Ang and P.J. Dyson, *Eur. J. Med. Chem.*, 4003 (2006); https://doi.org/10.1002/ejic.200600723.
11. S. Kathiresan, S. Mugesh, J. Annaraj and M. Murugan, *New J. Chem.*, **41**, 1267 (2017); https://doi.org/10.1039/C6NJ03501A.
12. A.A. Alothman, E.S. Al-Farraj, W.A. Al-Onazi, Z.M. Almarhoon and A.M. Al-Mohaimeed, *Arab. J. Chem.*, (2019); https://doi.org/10.1016/j.arabjc.2019.02.003.
13. F. Mohammadtabar, B. Shafaatian, A. Soleymanpour, S.A. Rezvani and B. Notash, *Transition Met. Chem.*, **41**, 475 (2016); https://doi.org/10.1007/s11243-016-0043-6.
14. T. Thirunavukkarasu, H.A. Sparkes, V.G. Gnanasoundari and K. Natarajan, *Appl. Organomet. Chem.*, **32**, 4403 (2018); https://doi.org/10.1002/aoc.4403.
15. R. Fekri, M. Salehi, A. Asadi and M. Kubicki, *Inorg. Chim. Acta*, **484**, 245 (2019); https://doi.org/10.1016/j.ica.2018.09.022.
16. A. Kamal, G. Bharath Kumar, V. Lakshma Nayak, V.S. Reddy, A.B. Shaik, R. Rajender and M. Kashi Reddy, *MedChemComm*, **6**, 606 (2015); https://doi.org/10.1039/C4MD00400K.
17. E. Kupeli, N. Erdemoglu, E. Yesilada and B. Sener, *J. Ethnopharmacol.*, **89**, 265 (2003); https://doi.org/10.1016/j.jep.2003.09.005.
18. H.H. Al-Rasheed, E.N. Sholkamy, M. Al Alshaikh, M.R.H. Siddiqui, A.S. Al-Obaidi and A. El-Faham, *J. Chem.*, **2018**, Article ID 8507567 (2018); https://doi.org/10.1155/2018/8507567.
19. P. Subbaraj, A. Ramu, N. Raman and J. Dharmaraja, *J. Saudi Chem. Soc.*, **19**, 207 (2015); https://doi.org/10.1016/j.jscs.2014.05.002.
20. K. Kiranmai, Y. Prashanthi and N.J.P. Subhashini, *J. Chem. Pharm. Res.*, **2**, 375 (2010).
21. L. Ruiz-Azuara and M. E. Bravo-Gomez, *Curr. Med. Chem.*, **17**, 3606 (2010); https://doi.org/10.2174/092986710793213751.
22. B.L. Vallee and D.S. Auld, *Biochemistry*, **29**, 5647 (1990); https://doi.org/10.1021/bi00476a001.
23. Y. Li, Z. Yang, M. Zhou, J. He, X. Wang, Y. Wu and Z. Wang, *J. Mol. Struct.*, **1130**, 818 (2017); https://doi.org/10.1016/j.molstruc.2016.10.092.
24. T. Todorovic, S. Grubisic, M. Pregelj, M. Jagodiè, S. Misirlic-Denèic, M. Dulovic, I. Markovic, O. Klisuric, A. Malesevic, D. Mitic, K. Andelkovic and N. Filipovic, *Eur. J. Inorg. Chem.*, **2015**, 3921 (2015); https://doi.org/10.1002/ejic.201500349.

25. T. Ito, S. Thyagarajan, K.D. Karlin and S.E. Rokita, *Chem. Commun.*, 4812 (2005); https://doi.org/10.1039/b509690a.
26. D.S. Goodman, *J. Am. Chem. Soc.*, **80**, 3802 (1958); https://doi.org/10.1021/ja01547a091.
27. E.L. Gelamo, C.H.T.P. Silva, H. Imasato and M. Tabak, *Biochim. Biophys. Acta*, **1594**, 84 (2002); https://doi.org/10.1016/S0167-4838(01)00287-4.
28. M. Xu, Z.R. Ma, L. Huang, F.J. Chen and Z.Z. Zeng, *Spectrochim. Acta A: Mol. Biomol. Spectrosc.*, **78**, 503 (2011); https://doi.org/10.1016/j.saa.2010.11.018.
29. M. Sedighipoor, A.H. Kianfar, W.A. Kamil Mahmood and M.H. Azarian, *Polyhedron*, **129**, 1 (2017); https://doi.org/10.1016/j.poly.2017.03.027.
30. M. Jiang, Y.-T. Li, Z.-Y. Wu, Z.-Q. Liu and C.-W. Yan, *J. Inorg. Biochem.*, **103**, 833 (2009); https://doi.org/10.1016/j.jinorgbio.2009.02.007.
31. A.P. Vieira, C.A. Wegermann and A.M. Da Costa Ferreira, *New J. Chem.*, **42**, 13169 (2018); https://doi.org/10.1039/C7NJ04799A.
32. S. Sujarani and A. Ramu, *J. Mol. Struct.*, **1079**, 353 (2015); https://doi.org/10.1016/j.molstruc.2014.08.041.
33. S. Sujarani and A. Ramu, *J. Mol. Struct.*, **1059**, 299 (2014); https://doi.org/10.1016/j.molstruc.2013.11.038.
34. P. Nithya, S. Helena, J. Simpson, M. Ilanchelian, A. Muthusankar and S. Govindarajan, *J. Photochem. Photobiol. B*, **165**, 220 (2016); https://doi.org/10.1016/j.jphotobiol.2016.10.024.
35. M. Sakthi and A. Ramu, *J. Mol. Struct.*, **1149**, 727 (2017); https://doi.org/10.1016/j.molstruc.2017.08.040.
36. L.H. Abdel-Rahman, M.S.S. Adam, A.M. Abu-Dief, H. Moustafa, M.T. Basha, A.S. Aboraia, B.S. Al-Farhan and H. El-Sayed Ahmed, *Appl. Organomet. Chem.*, **32**, e4527 (2018); https://doi.org/10.1002/aoc.4527.
37. T. Sarkar, S. Banerjee, S. Mukherjee and A. Hussain, *Dalton Trans.*, **45**, 6424 (2016); https://doi.org/10.1039/C5DT04775G.
38. N. Shahid, N. Sami, M. Shakir and M. Aatif, *J. Saudi Chem. Soc.*, **23**, 315 (2019); https://doi.org/10.1016/j.jscs.2018.08.004.
39. N.B. Gopal Reddy, P.M. Krishna, S.S. Shantha Kumar, Y.P. Patil and M. Nethaji, *J. Mol. Struct.*, **1137**, 543 (2017); https://doi.org/10.1016/j.molstruc.2017.02.009.
40. M.C. Mandewale, B. Thorat, Y. Nivid, R. Jadhav, A. Nagarsekar and R. Yamgar, *J. Saudi Chem. Soc.*, **22**, 218 (2018); https://doi.org/10.1016/j.jscs.2016.04.003.
41. S.Y. Ebrahimipour, I. Sheikhshoaie, M. Mohamadi, S. Suarez, R. Baggio, M. Khaleghi, M. Torkzadeh-Mahani and A. Mostafavi, *Spectrochim. Acta A Mol. Biomol. Spectrosc.*, **142**, 410 (2015); https://doi.org/10.1016/j.saa.2015.01.088.
42. U.L. Kala, S. Suma, M.R.P. Kurup, S. Krishnan and R.P. John, *Polyhedron*, **26**, 1427 (2007); https://doi.org/10.1016/j.poly.2006.11.035.
43. S.T. Chew, K.M. Lo, S.K. Sinniah, K.S. Sim and K.W. Tan, *RSC Adv.*, **4**, 61232 (2014); https://doi.org/10.1039/C4RA11716F.
44. C. Gokce and R. Gup, *Appl. Organomet. Chem.*, **27**, 263 (2013); https://doi.org/10.1002/aoc.2955.
45. M. Kumar, S. Roy, M.S.H. Faizi, S. Kumar, M.K. Singh, S. Kishor, S.C. Peter and R.P. John, *J. Mol. Struct.*, **1128**, 195 (2017); https://doi.org/10.1016/j.molstruc.2016.08.004.
46. C.J. Dhanaraj and M.S. Nair, *J. Saudi Chem. Soc.*, **18**, 479 (2014); https://doi.org/10.1016/j.jscs.2011.10.006.
47. M.C. linescu, M.L. Fiastru, D. Bala, C. Mihailciuc, T.N. Pýrjol and B. Jurca, *J. Saudi Chem. Soc.*, (2019) (in press); https://doi.org/10.1016/j.jscs.2019.02.006.
48. K. Nagashri, J. Joseph and C.J. Dhanaraj, *Arab. J. Chem.*, **9**, 548 (2016); https://doi.org/10.1016/j.arabjc.2011.06.027.
49. S. Yadav, I. Yousuf, M. Usman, M. Ahmad, F. Arjmand and S. Tabassum, *RSC Adv.*, **5**, 50673 (2015); https://doi.org/10.1039/C5RA06953J.
50. N. Raman, R. Mahalakshmi, T. Arun, S. Packianathan and R. Rajkumar, *J. Photochem. Photobiol. B*, **138**, 211 (2014); https://doi.org/10.1016/j.jphotobiol.2014.05.018.
51. S. Kathiresan, T. Anand, S. Mugesh and J. Annaraj, *J. Photochem. Photobiol. B*, **148**, 290 (2015); https://doi.org/10.1016/j.jphotobiol.2015.04.016.
52. S. Kathiresan, S. Mugesh, M. Murugan, F. Ahamed and J. Annaraj, *RSC Adv.*, **6**, 1810 (2016); https://doi.org/10.1039/C5RA20607C.
53. V.M. Manikandamathavan, T. Weyhermuller, R.P. Parameswari, M. Sathishkumar, V. Subramanian and B.U. Nair, *Dalton Trans.*, **43**, 13018 (2014); https://doi.org/10.1039/C4DT01378F.
54. L. Li, Q. Guo, J. Dong, T. Xu and J. Li, *J. Photochem. Photobiol. B*, **125**, 56 (2013); https://doi.org/10.1016/j.jphotobiol.2013.05.007.
55. S. Banerjee, S. Mondal, W. Chakraborty, S. Sen, R. Gachhui, R.J. Butcher, A.M.Z. Slawin, C. Mandal and S. Mitra, *Polyhedron*, **28**, 2785 (2009); https://doi.org/10.1016/j.poly.2009.05.071.
56. P. Kavitha, M. Rama Chary, B.V.V.A. Singavarapu and K. Laxma Reddy, *J. Saudi Chem. Soc.*, **20**, 69 (2016); https://doi.org/10.1016/j.jscs.2013.03.005.
57. M.S. Nair, D. Arish and R.S. Joseyphus, *J. Saudi Chem. Soc.*, **16**, 83 (2012); https://doi.org/10.1016/j.jscs.2010.11.002.
58. N. Raman, S. Sobha and L. Mitu, *Monatsh. Chem.*, **143**, 1019 (2012); https://doi.org/10.1007/s00706-011-0699-8.
59. S.S. Sreejith, N. Mohan and M.R.P. Kurup, *Polyhedron*, **135**, 278 (2017); https://doi.org/10.1016/j.poly.2017.07.015.
60. D. Senthil Raja, E. Ramachandran, N.S.P. Bhuvanesh and K. Natarajan, *Eur. J. Med. Chem.*, **64**, 148 (2013); https://doi.org/10.1016/j.ejmech.2013.03.040.
61. P. Krishnamoorthy, P. Sathyadevi, R.R. Butorac, A.H. Cowley, N.S.P. Bhuvanesh and N. Dharmaraj, *Dalton Trans.*, **41**, 4423 (2012); https://doi.org/10.1039/c2dt11938b.
62. M. Das, B. Kumar Kundu, R. Tiwari, P. Mandal, D. Nayak, R. Ganguly and S. Mukhopadhyay, *Inorg. Chim. Acta*, **469**, 111 (2018); https://doi.org/10.1016/j.ica.2017.09.013.
63. K. Hu, F. Li, Z. Zhang and F. Liang, *New J. Chem.*, **41**, 2062 (2017); https://doi.org/10.1039/C6NJ02483A.
64. P. Vijayan, P. Viswanathamurthi, K. Velmurugan, R. Nandhakumar, M.D. Balakumaran, P.T. Kalaichelvan and J.G. Malecki, *RSC Adv.*, **5**, 103321 (2015); https://doi.org/10.1039/C5RA18568H.